

Durham Research Online

Deposited in DRO:

21 September 2021

Version of attached file:

Published Version

Peer-review status of attached file:

Peer-reviewed

Citation for published item:

Khoze, V. A. and Martin, A. D. and Ryskin, M. G. (2021) 'Dynamics of diffractive dissociation.', The European Physical Journal C, 81 (2).

Further information on publisher's website:

<https://doi.org/10.1140/epjc/s10052-021-08953-9>

Publisher's copyright statement:

Open Access This article is licensed under a Creative Commons Attribution 4.0 International License, which permits use, sharing, adaptation, distribution and reproduction in any medium or format, as long as you give appropriate credit to the original author(s) and the source, provide a link to the Creative Commons licence, and indicate if changes were made. The images or other third party material in this article are included in the article's Creative Commons licence, unless indicated otherwise in a credit line to the material. If material is not included in the article's Creative Commons licence and your intended use is not permitted by statutory regulation or exceeds the permitted use, you will need to obtain permission directly from the copyright holder. To view a copy of this licence, visit <http://creativecommons.org/licenses/by/4.0/>.

Additional information:

Use policy

The full-text may be used and/or reproduced, and given to third parties in any format or medium, without prior permission or charge, for personal research or study, educational, or not-for-profit purposes provided that:

- a full bibliographic reference is made to the original source
- a [link](#) is made to the metadata record in DRO
- the full-text is not changed in any way

The full-text must not be sold in any format or medium without the formal permission of the copyright holders.

Please consult the [full DRO policy](#) for further details.



Dynamics of diffractive dissociation

V. A. Khoze^{1,2}, A. D. Martin^{1,a}, M. G. Ryskin^{1,2}

¹ Institute for Particle Physics Phenomenology, University of Durham, Durham DH1 3LE, UK

² Petersburg Nuclear Physics Institute, NRC Kurchatov Institute, Gatchina, St. Petersburg 188300, Russia

Received: 18 December 2020 / Accepted: 4 February 2021 / Published online: 22 February 2021

© The Author(s) 2021

Abstract We describe a QCD based model which incorporates the main properties of the inclusive particle distributions expected for diffractive processes, including the diffractive dissociation at high energies. We study, in turn, the total cross section, σ_{tot} , the differential elastic, $d\sigma_{\text{el}}/dt$, cross section, the dependence of the single proton dissociation cross section, $\xi d\sigma^{\text{SD}}/d\xi$, on the momentum fraction, $\xi = 1 - x_L$, lost by the leading proton, the multiplicity distributions in inelastic (non-diffractive) collisions and in the processes of dissociation. Besides this we calculate the mean transverse momenta of the ‘wee partons’ (secondaries) produced in the case of dissociation (that is in the processes with a large rapidity gap) and compare it with that in inelastic interactions.

1 Introduction

In a recent paper [1] the inclusive distribution of identified particles produced in Single Diffractive Dissociation (SD) $pp \rightarrow p + X$ processes were studied with the STAR detector at RHIC in proton–proton collisions at $\sqrt{s} = 200$ GeV. Here X denotes the diffractively produced system. The SD events were selected by observing in the Roman Pot system(s) the leading proton (or protons) which carry a large fraction, x_L , of the beam momentum. We denote $x_L = 1 - \xi$. Analogous experiments are underway or being planned by CMS-TOTEM (PPS) and ATLAS-AFP at the LHC. The leading proton is observed in the TOTEM or ALFA Roman Pots while the diffracted system X is studied by the central CMS or ATLAS detectors (see e.g. [2, 3]).

Note that after the leading proton(s) with large x_L close to 1 are detected we have rather small remaining energy to produce the new secondaries. Therefore, these new secondaries (system X) are separated from the leading proton(s) by Large

Rapidity Gap(s) (LRG) with size¹ $\Delta y \simeq \ln(1/\xi)$. Since the interaction across the LRG is provided by the Pomeron exchange such events can be interpreted as the result of a Pomeron interaction with a proton (SD). The processes are illustrated in Fig. 1a.

In the first approximation at large mass, M_X , of the system X the Pomeron–proton interaction is driven by another Pomeron exchange and the cross section of whole process is described by the triple-Pomeron diagram Fig. 1b.

However actually the situation is more complicated and the simple triple-Pomeron diagram can be used only in the situation when the probability of interaction is relatively small and the parton densities are rather low. On another hand diffractive dissociation is a soft process and here we deal with *strong* interactions. Therefore we have to consider the possibility of a few simultaneous interactions. Indeed, there is a rather large probability that the LRG will be filled by secondaries produced in an additional soft interaction² and instead of single proton dissociation (SD) we will observe a completely inelastic event. That is we have to account for the gap survival probability, $S^2 < 1$, which in terms of the Reggion Field Theory [4] is described by the multi-Pomeron diagrams responsible for the absorptive corrections. For this reason the distributions of particles produced in non-diffractive inelastic collisions and in the processes with LRG become different.

At a qualitative level the corresponding difference was discussed in [5]. In the present paper we consider a model which allows us to evaluate the expected difference (semi)quantitatively. We attempt to make our model relatively simple, but to keep the main properties of the develop-

¹ For $pp \rightarrow p + X$ the mass M_X of the produced system X is given by $M_X^2 = s(1 - x_L)$ with gap sizes $\Delta y \simeq -\ln(1 - x_L)$.

² In Monte Carlo Models this is called the Multiple Parton Interaction option (MPI). Recall that in the present paper we consider only an *individual* pp -collision and do not account for the possibility of other proton–proton interactions in the same bunch crossing which occur if the instantaneous luminosity is large.

^a e-mail: a.d.martin@durham.ac.uk (corresponding author)

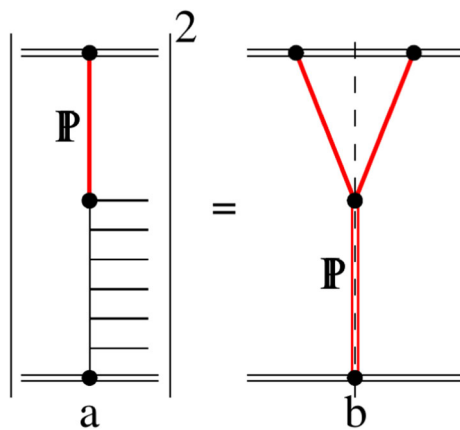


Fig. 1 Schematic diagrams of single diffractive (SD) processes in Pomeron–proton collisions

ment of the ‘wee parton’ cascade;³ namely we account for the ‘diffusion’ in impact parameter, b , space and for the growth of the characteristic transverse momenta, k_t , when the parton density becomes large. These are the important features of the perturbative QCD evolution observed within the BFKL [8–14] and multi-Pomeron approach (see e.g. [15, 16] and for a recent review [17]).

Recall that within perturbative QCD, the BFKL equation describes the rapidity (y) evolution of parton/gluon density (i.e. the proton opacity, $\Omega(y)$) and predicts the exponential growth $\Omega(y) \propto \exp(\omega_{\text{BFKL}} y)$. Moreover, at each step of the evolution the parton transverse momentum, k_t , may be changed few times in one or another direction and the position of a parton in impact parameter space, b , can be moved by $\Delta b \sim 1/k_t$. That is we have diffusion in both the b and $\ln k_t$ spaces. The absorptive corrections make this diffusion asymmetric. Due to a larger parton density, and correspondingly to stronger absorptive corrections, in the centre of disk the partons are mainly moving in the direction of the periphery; while the remaining partons occupy the larger k_t elements of the (b, k_t) configuration space (see sect. 3.2 of [16] for more details).

Looking for events with a LRG we select interactions occurring in the periphery of the disk where the probability of gap survival is larger. Thus in order to reproduce the main feature of diffractive dissociation at high energies our model must include

- the growth of parton densities,
- the possibility of movement in b -plane,
- absorptive corrections during the y -evolution process,

³ We use the term ‘wee parton’ in the spirit of Feynman and Gribov [6, 7] as some elementary object which participates in strong interactions and carries a very small part of the parent hadron momentum. In the case of QCD it is mainly the gluon. However in our simplified model we do not fix the quantum numbers of these partons.

- gap survival probabilities with respect to the rescattering of the partons which belong to the different (beam and target) incoming protons.

In the next section we describe the structure of the evolution of the ‘wee-parton’ cascade. Then in Sect. 3 we present the formulae to calculate the total, elastic and diffractive dissociation cross sections and the multiplicity distributions of secondaries based on the resulting cascades. Numerical values of parameters used in the model are presented in Sect. 4, while in Sect. 5 we show the results obtained for SD processes. These results will be discussed in Sect. 6. We conclude in Sect. 7.

2 Parton evolution

Describing the evolution of the wee-parton cascade we will account for the absorptive effects caused by the possibility of an additional interaction between the parton and the parent proton.⁴ That is, our approach includes not only the multiple interactions between the beam and target hadrons (protons) but also the multiple interactions between the particular parton and the proton as well. For this purpose we use the eikonal model. That is, we assume an eikonal-like form of the multi-Pomeron vertices. Specifically the coupling of n to m Pomerons takes the form

$$g_m^n = (g_N \lambda)^{n+m-2}, \quad (1)$$

where g_N is the proton–Pomeron coupling and λ accounts for the suppression of the triple-Pomeron vertex ($g_{3P} = g_2^1$) in comparison with g_N .

2.1 Good–Walker formalism

In the simplest case we have a one-channel eikonal model in which at hadron level we consider only elastic (intact proton) intermediate states. To allow for the possibility of low mass $p \rightarrow N^*$ excitations (in the intermediate state), we need a multi-channel eikonal with g_{pN^*} and $g_{N_a^* N_b^*}$ transition vertices. For this we use the Good–Walker (G–W) formalism [18] which introduces states ϕ_k that diagonalize the T matrix of the high energy hadrons couplings (e.g. in the proton case describes different $p \rightarrow N^*$, $N_a^* \rightarrow N_b^*$ transitions). Such eigenstates only undergo elastic scattering since there are no off-diagonal transitions. That is

$$\langle \phi_i | T | \phi_k \rangle = 0 \quad \text{for } i \neq k \quad (2)$$

and so a state k cannot diffractively dissociate in to a state i . Thus, working in terms of G–W eigenstates ϕ_i , we have

⁴ We ignore here the parton–parton rescatterings. These give a smaller effect.

a simple one-channel eikonal for each state. We denote the orthogonal matrix which diagonalizes $\text{Im } T$ by a , so that

$$\text{Im } T = a F(a)^T \quad \text{with} \quad \langle \phi_i | F | \phi_k \rangle = F_k \delta_{ik}, \quad (3)$$

where F_k is the probability of the hadronic process proceeding via the diffractive eigenstate ϕ_k .

Now consider the diffractive dissociation of an incoming state $|i\rangle$. We can write

$$|i\rangle = \sum_k a_{ik} |\phi_k\rangle. \quad (4)$$

The elastic scattering amplitude satisfies

$$\langle i | \text{Im } T | i \rangle = \sum_k |a_{ik}|^2 F_k = \langle F \rangle, \quad (5)$$

where $F_k \equiv \langle \phi_k | F | \phi_k \rangle$. Here the brackets of $\langle F \rangle$ mean that we take the average of F over the initial probability distribution of diffractive eigenstates. After diffractive scattering described by G_{fi} , the final state $|f\rangle$ will, in general, be a different superposition of eigenstates from that of the initial state $|i\rangle$, which was shown in (4). Neglecting the real parts of the amplitudes for the moment, the cross sections at a given impact parameter b , will have the forms

$$\frac{d\sigma_{\text{tot}}}{d^2b} = 2 \text{Im} \langle i | T | i \rangle = 2 \sum_k |a_{ik}|^2 F_k = 2 \langle F \rangle \quad (6)$$

$$\frac{d\sigma_{\text{el}}}{d^2b} = |\langle i | T | i \rangle|^2 = \left(\sum_k |a_{ik}|^2 F_k \right)^2 = \langle F \rangle^2 \quad (7)$$

$$\frac{d\sigma_{\text{el}} + \text{SD}}{d^2b} = \sum_k |\langle \phi_k | T | \phi_i \rangle|^2 = \sum_k |a_{ik}|^2 F_k^2 = \langle F^2 \rangle. \quad (8)$$

It follows that the cross section for the single diffractive dissociation of a proton,

$$\frac{d\sigma_{\text{SD}}}{d^2b} = \langle F^2 \rangle - \langle F \rangle^2, \quad (9)$$

is given by the statistical dispersion in the absorption probabilities of the diffractive eigenstates. Here the average is taken over the components k of the incoming proton which dissociates.

One consequence is the important result that if all the components ϕ_k of the incoming proton $|i\rangle$ were absorbed equally then the diffracted superposition would be proportional to the incident one and the inelastic diffraction would be zero. Thus if, at very high energies, the amplitudes F_k at small impact parameters are equal to the black disk limit, $F_k = 1$, then diffractive production will be equal to zero in this impact parameter domain, and so the dissociation will only occur in the peripheral b region where the edge of the disk is not completely black. Hence the impact parameter structure of diffractive dissociation and elastic scattering are drastically

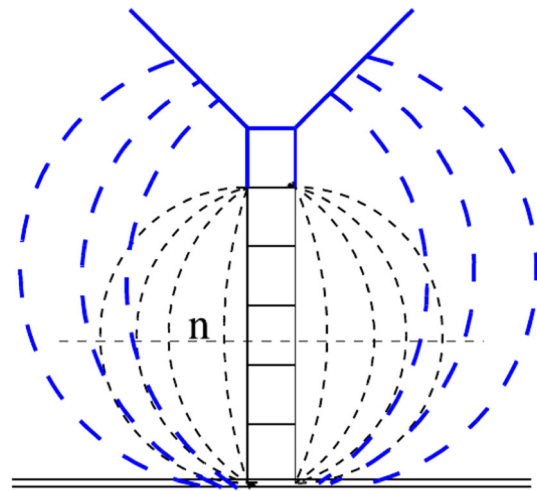


Fig. 2 Evolution of the wee parton density in rapidity (momentum fraction) space. The last step of evolution is shown by thick (blue) lines. The dashed curves indicate the eikonal-like absorptive corrections. n is the number of screening Pomerons

different in the presence of absorptive s -channel unitarity effects.

In our simple model to account for the low mass dissociation⁵ we will include two eigenstates which at the beginning of evolution ($y = 0$) have different sizes, that is different impact parameter, b distributions of the parton densities, but almost equal densities at $b = 0$. To minimize the number of free parameters these two eigenstates are taken with equal probabilities, that is $a_{p1} = a_{p2} = 1/\sqrt{2}$.

2.2 Rapidity evolution

Here we consider the evolution in rapidity y of the parton cascade generated by an individual G–W eigenstate. To describe the evolution of the wee parton density in rapidity space we first neglect the diffusion in impact parameter, b , and omit the absorptive effects. For a fixed b the optical density (opacity), $\Omega(b, y)$ evolves with decreasing momentum fraction, x , carried by the parton as

$$\frac{d\Omega(b, y)}{dy} = \Delta\Omega(b, y) \quad y = \ln(1/x), \quad (10)$$

where we expect that the value of Δ to be close to that (ω_{BFKL}) given by the BFKL [8–14] intercept ω_{BFKL} . That is accounting for (and re-summing) the next-to-leading logarithm corrections we expect $\Delta \sim 0.15 - 0.25$ [19–23]. This evolution is indicated by the continuous lines in Fig. 2, where the thick (blue) lines indicate the last step of the evolution in y .

At each step of the evolution we have to account for the absorptive effects caused by additional parton-target inter-

⁵ The high mass, M_X , dissociation will be described in Sect. 3.

actions which are shown in Fig. 2 by dashed curves. It is convenient now to deal with the probability of an inelastic interaction G rather than with the opacity Ω

$$G(b, y) = 1 - e^{-\Omega(b, y)}. \quad (11)$$

Here we assume an eikonal form of the multi-Pomeron vertices. Each step of the evolution is now suppressed by the survival factor $\exp(-\Omega) = 1 - G(b, y)$ and the evolution reads

$$\frac{dG(b, y)}{dy} = \Delta(1 - G(b, y)) G(b, y). \quad (12)$$

The factor $(1 - G(b, y))$ provides the saturation of the parton density as $G \rightarrow 1$.⁶

Next we have to include the diffusion in the transverse b -plane.⁷ This is an important effect which leads to the shrinkage of the diffractive cone (i.e. to the growth of the elastic t -slope, B_{el} , with energy). At each step of the evolution the parton can move in b space by some interval $\delta b \simeq 1/k_t$, where k_t is the parton transverse momentum.

Actually the main effect is observed when the parton moves *outwards* from the centre of disk. Only this will be accounted for in our simplified model. We assume that one quarter (one of the four $(+x, -x, +y, -y)$ possible transverse directions) of the partons generated at each step of the evolution goes to a larger value of b with probability⁸

$$\frac{dP(b)}{db} = k_t(b) \exp(-bk_t(b)), \quad (13)$$

where we consider only the movement outside of the centre of the disk and $k_t(b)$ is the typical transverse momentum of the parton placed at impact parameter b . That is finally we obtain the evolution equation

$$\begin{aligned} \frac{dG(b, y)}{dy} = (1 - G(b, y)) & \left[\frac{3}{4} \Delta G(b, y) \right. \\ & \left. + \frac{1}{4} \Delta \int_0^b db' G(b', y) k_t(b', y) e^{(b'-b)k_t(b', y)} \right]. \end{aligned} \quad (14)$$

This should be complemented by the equation for $k_t(b, y)$. As far as the parton density approaches its saturation limit ($G \rightarrow 1$) the new partons start to occupy a larger k_t region.

⁶ In general the parton density, $D(y, b, k_t)$, depends on three arguments – y , b and k_t . In the present simplified model we do not include the k_t dependence explicitly. Instead we evaluate the mean value $\langle k_t \rangle$ at each (y, b) point. Thus the function $G(y, b) = \int D(y, b, k_t) d \ln(k_t)$ accounts for the probability of the interaction with a parton at the point (y, b) independent of the parton transverse momentum (i.e. integrated over k_t).

⁷ The diffusion in b space was considered long ago in [24, 25].

⁸ A more detailed description of the diffusion in b space can be found in section 2.4 of [16], where it is shown that the typical size of the diffusion step is $\Delta b \simeq 1/k_t$.

Asymptotically we have to keep the probability of an additional interaction $w = \sigma^{\text{abs}}/\pi R^2 = \text{const}$. Here πR^2 is the “hot spot” area occupied by the parton cascade. In the first approximation the absorptive cross section σ^{abs} increases with $y = \ln(1/x)$ as $\sigma^{\text{abs}} \propto (1/k_t^2) \exp(y\Delta)$. That is the transverse momentum k_t grows as $k_t \propto \exp(y\Delta/2)$. Being far from the saturation limit we expect more or less constant k_t but when the density $G \rightarrow 1$ approaches saturation the value of k_t starts to grow. Therefore we choose

$$\frac{dk_t(b, y)}{dy} = \frac{\Delta}{2} k_t(b, y) G(b, y). \quad (15)$$

These two Eqs. (14) and (15) describe our simplified evolution of the wee parton cascade. When the parton density is small ($G \ll 1$) the new partons created at the current step of evolution have more or less the same k_t as the parent parton and mainly enlarge the value of $G(b)$ at the same b point, partly moving to the periphery of disk; that is, to larger b . At a larger density G this process is suppressed by the $1 - G(b)$ factor. The ‘remaining’ partons (see the last factor G in (15)) start to occupy a larger k_t space (see [16] for a more detailed description of the parton cascade development).

The b dependence of $G(b, y)$ and $k_t(b, y)$ at a few values of $y = 3, 6$ and 9 generated by this model is shown in Fig. 3 where we have used the parameters tuned to describe the total and elastic $p\bar{p}$ and pp cross sections in the $Sp\bar{p}S$, Tevatron and the LHC colliders energy range, as described in Sect. 4.

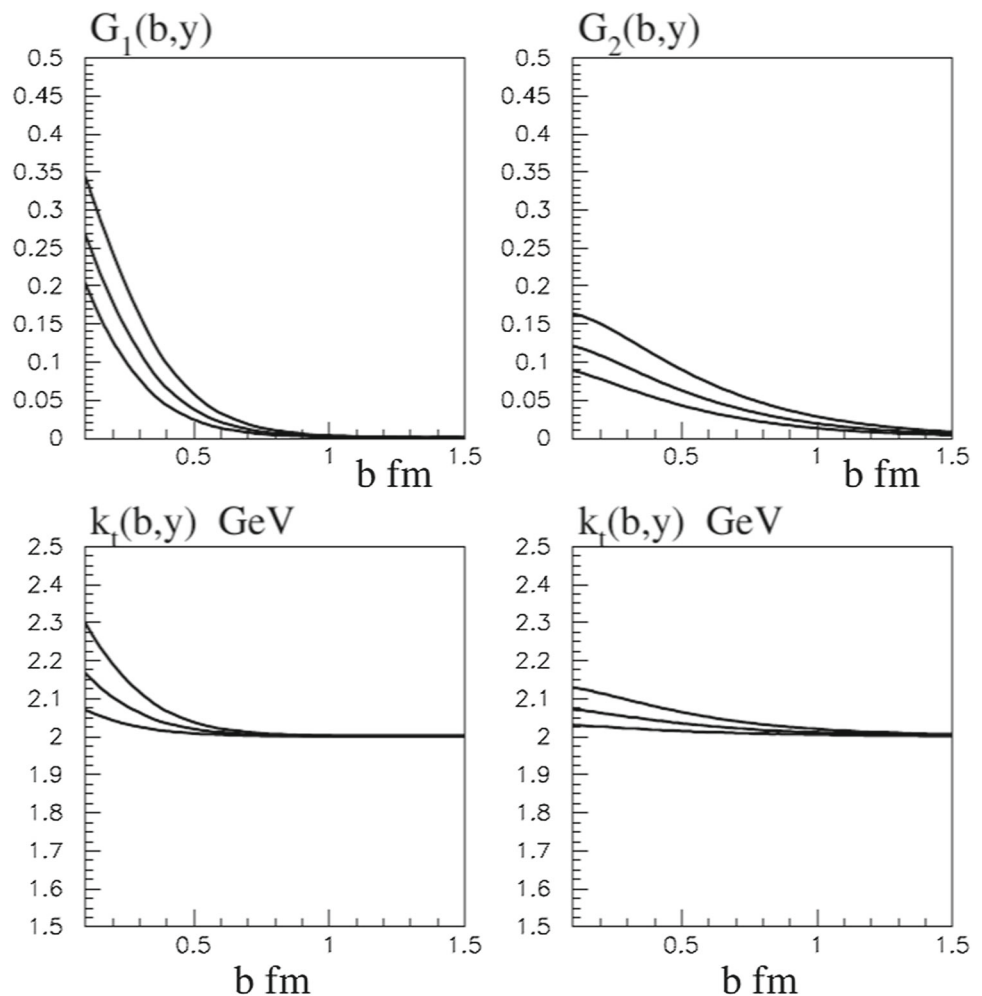
3 Formulae for observables

To calculate the cross section of the high energy proton–proton interaction we have to consider the collision of the two parton cascades generated by the incoming beam and target hadrons. We start with the collision of the i and j G–W components at rapidity y_1 . The effective opacity Ω_{ij} is given by

$$\begin{aligned} \Omega_{ij}(b_{ij}, Y; y_1) = \int d^2b_1 d^2b_2 G_i(b_1, y_1) \frac{1}{\sigma_0} G_j(b_2, y_2) \delta^{(2)} \\ \times (\mathbf{b}_{ij} - \mathbf{b}_1 + \mathbf{b}_2), \end{aligned} \quad (16)$$

where b_{ij} is the transverse separation (impact factor) between the two colliding protons and $y_1 + y_2 = Y = \ln s$ is the full rapidity interval between the beam and target hadrons. The dimensionful factor σ_0 accounts for the cross section of the elementary parton–parton interaction. Recall that at the beginning of the evolution the probability, $G(b)$, to find a parton at point b was proportional to σ_0 . Therefore to cancel the extra σ_0 we are required to have σ_0 in denominator of (16).

Fig. 3 Impact parameter, b , dependence of the parton densities, $G_i(b, y)$ (upper panels) and the characteristic transverse momenta, $k_{ti}(b, y)$ (lower panels) for the two G-W components, $|\phi_1\rangle$ (left) and $|\phi_2\rangle$ (right) at three values of rapidity $y = 9, 6, 3$ – the curves from top to bottom. We use the values of the parameters which have been tuned to describe the total and elastic $p\bar{p}$ and pp cross sections in the $Sp\bar{p}S$, Tevatron and the LHC colliders energy range



3.1 Total and elastic cross sections

The elastic scattering amplitude reads

$$A_{ij}(b) = i \left(1 - e^{-\Omega_{ij}(b)/2} \right) \quad (17)$$

leading to a total cross section

$$\sigma_{\text{tot}} = 2 \int d^2b \sum_{ij} |a_i|^2 |a_j|^2 \left(1 - e^{-\Omega_{ij}(b)/2} \right) \quad (18)$$

and a differential elastic cross section

$$\frac{d\sigma_{\text{el}}}{dt} = \frac{1}{4\pi} \left| \int d^2b e^{i\mathbf{q}_t \cdot \mathbf{b}} \times \sum_{i,j} |a_i|^2 |a_j|^2 \left(1 - e^{-\Omega_{ij}(b)/2} \right) \right|^2, \quad (19)$$

where $t = -|\mathbf{q}_t|^2$. The t slope of the elastic cross section B_{el} at $t = 0$ can be calculated as the mean $\langle b^2 \rangle$. That is

$$B_{\text{el}}(t=0) = \frac{\left| \int d^2b b^2 \sum_{i,j} |a_i|^2 |a_j|^2 \left(1 - e^{-\Omega_{ij}(b)/2} \right) \right|^2}{\left| \int d^2b \sum_{i,j} |a_i|^2 |a_j|^2 \left(1 - e^{-\Omega_{ij}(b)/2} \right) \right|^2}. \quad (20)$$

Formally the result should not depend on the rapidity y_1 at which the collision of the two parton cascades was calculated. Our simplified model does not fulfill this condition exactly.⁹ However the results do not depend too much on the particular y_1 value. If, for example, instead of the usual $y_1 = y_2 = Y/2$ we take $y_1 = Y/8$ and $y_2 = 7Y/8$ then the values of σ_{tot} change by less than 6% and the elastic slope B_{el} by less than 1%.

Up to now we have calculated just the imaginary part of the amplitude. Since we are dealing with the even-signature amplitude¹⁰ the real part can be restored via dispersion rela-

⁹ In terms of Reggeon Field Theory the remaining y_1 dependence is caused by the fact that in the present model we neglect part of the enhanced and some specific semi-enhanced (Pomeron loop) diagrams.

¹⁰ The odd-signature contributions are not included in the evolution.

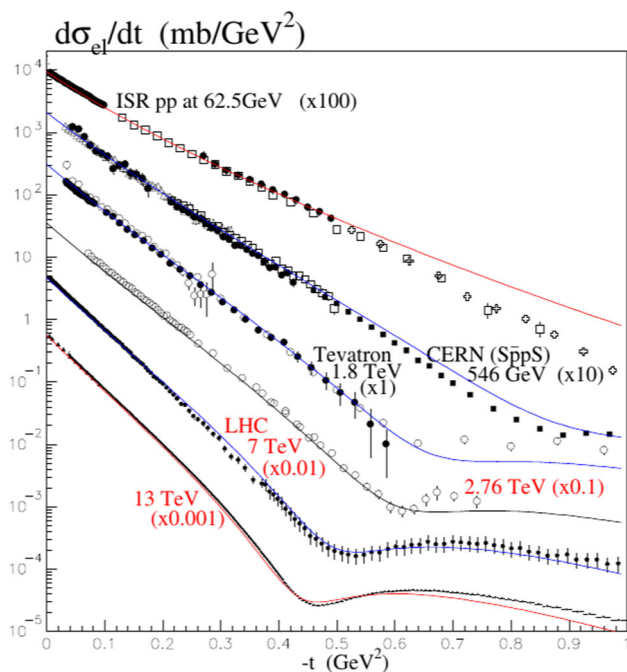


Fig. 4 The t dependence of the elastic proton–proton (proton–antiproton) cross sections in the $S\bar{p}pS$, Tevatron and the LHC colliders energy range. The parameters of model were tuned as described in Sect. 4. The data are taken from [33–46]. The poor description of the data at the larger values of $-t$ can be improved by using a more detailed G–W parameterization, but this is not relevant to our study

tions. In our high energy limit we use it for fixed b (i.e. for a fixed partial wave with orbital angular momentum $l = b\sqrt{s}/2$) in the simplified form

$$\text{Re}A(b, s) = \frac{\pi}{2} \frac{\partial \text{Im}A(b, s)}{\partial \ln s}. \quad (21)$$

This real part has been included in the results presented in Fig. 4.

3.2 High-mass diffractive dissociation

To obtain the cross section of diffractive dissociation we have to consider the case where in the rapidity interval from y_1 to Y we have elastic scattering (upper part of the diagram in Fig. 1) while below y_1 there is an inelastic process (in Fig. 1 it is shown by the lower central Pomeron). Besides this we have to include the gap survival factor, $\exp(-\Omega_{ij}/2)$ for the amplitude, to be sure that there are no additional inelastic interactions which may fill the gap.

The corresponding cross section takes the form

$$\begin{aligned} \frac{\xi d\sigma^{\text{SD}}}{d\xi} &= \frac{d\sigma^{\text{SD}}}{dy_1} \\ &= \int d^2b_1 \sum_j |a_j|^2 \frac{\lambda G_j(b_1, y_1)}{\sigma_0} d^2b_2 \end{aligned}$$

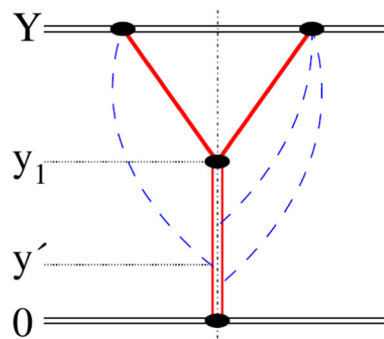


Fig. 5 Semi-enhanced diagrams (shown by the dashed blue lines) which describe the probability of LRG survival with respect to the interactions with the intermediate partons

$$\begin{aligned} &\cdot \left(\sum_i |a_i|^2 (1 - \sqrt{1 - G_i(b_2, y_2)}) e^{-\Omega_{ij}(b_1+b_2, Y)/2} S_i^{\text{enh}}(b_2, y_1) \right) \\ &\cdot \left(\sum_{i'} |a_{i'}|^2 (1 - \sqrt{1 - G_{i'}(b_2, y_2)}) e^{-\Omega_{i'j}(b_1+b_2, Y)/2} S_{i'}^{\text{enh}}(b_2, y_1) \right)^*, \end{aligned} \quad (22)$$

where $y_2 = Y - y_1$ and the ‘elastic’ amplitude $(1 - e^{-\Omega/2})$ generated by the parton cascade (in the upper part of Fig. 1), $G_i(b_2, y_2) = 1 - \exp(-\Omega_i(b_2, y_2))$ is written as $(1 - \sqrt{1 - G})$.

Recall that $\lambda = g_{3P}/g_N$ is the ratio of the triple-Pomeron to Pomeron-nucleon couplings. Its value determines the probability of interactions within a unit interval of rapidities. Thus λ is proportional to the parton density in rapidity evolution which in its turn is of the order of Δ .

Finally the factor $S_{ij}^{\text{enh}}(b_2, y_1)$ accounts for the probability of LRG survival with respect to soft interactions with the intermediate partons from the cut Pomeron¹¹ (in the lower part of Fig. 1). It is given by the sum of the enhanced diagrams (see the dashed blue lines in Fig. 5)

$$S_i^{\text{enh}}(b, y_1) = \exp \left(- \int_{1.6}^{y_1} dy' \frac{\lambda}{2} G_i(b, Y - y') \right). \quad (23)$$

Here we start the integration over y' from $y'_{\min} = 1.6$ since the interval of lower y' is already accounted for in terms of the G–W eigenstates.

Strictly speaking there should be the integration over the position of the new interaction point b in the impact parameter plane. However, since due to the large value of $k_0 \sim 2$ GeV (i.e. the small slope of the Pomeron trajectory α'_P) the diffusion in the b plane is rather weak, we put in (22) a fixed value of $b = b_2$.¹²

¹¹ ‘Cut’ denotes the Pomeron which produces the secondary hadrons (like that in the lower part of Fig. 1a) and not the Pomerons which describe the absorptive effects (like that shown by dashed curves in Fig. 2).

¹² This, second order, effect of the diffusion in the b plane should be accounted for in a future more precise version of the model.

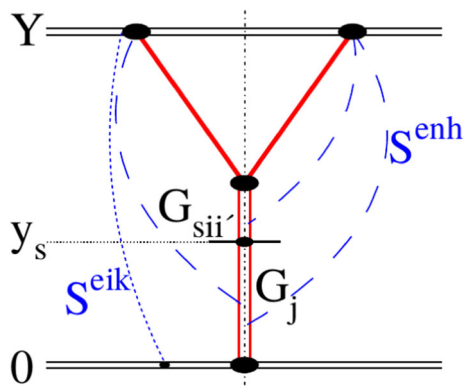


Fig. 6 The diagram for the inclusive one particle cross section for SD events. Screening effects are indicated by the (blue) short-dashed (S^{eik}) and (blue) long-dashed (S^{enh}) curves which describe the probability of LRG survival with respect to additional proton–proton interactions or the interactions with the intermediate partons

Next, the slope of diffractive dissociation $B_{\text{dis}}(t = 0) = \langle b_2^2 \rangle$ reads

$$B_{\text{dis}}(t=0) = \frac{\int d^2 b_1 \sum_j |a_j|^2 G_j(b_1, y_1) d^2 b_2 b_2^2 (\sum_i |a_i|^2 \dots) (\sum_{i'} |a_{i'}|^2 \dots)^*}{\int d^2 b_1 \sum_j |a_j|^2 G_j(b_1, y_1) d^2 b_2 (\sum_i |a_i|^2 \dots) (\sum_{i'} |a_{i'}|^2 \dots)^*}, \quad (24)$$

where ‘dots’ denote the corresponding expressions in the second and third lines of (22).

3.3 Density of secondaries in LRG events

The inclusive cross section of secondaries produced at rapidity y_s in the high-mass dissociation is (see Fig. 6)

$$\begin{aligned} \frac{\xi d\sigma^{\text{SD}}}{d\xi dy_s} &= \int d^2 b_1 d^2 b_s \sum_{iji'} |a_i^2| |a_{i'}^2| |a_j|^2 \\ &\times \frac{g_s G_j(b_1, y_s) G_{sii'}(b_s, y_3)}{\sigma_0} S_{ij}^{\text{eik}} S_{i'j}^{\text{eik}} S_{ii'}^{\text{enh}}(b_s, Y - y_{\text{gap}}), \end{aligned} \quad (25)$$

where the constant g_s is the probability of secondary particle emission from a one cut Pomeron.¹³ We put $g_s = 2.2$ in order to have the density of charged particles in non-diffractive events $dN_{\text{ch}}/dy = 6$ at $\sqrt{s} = 13$ TeV to be in agreement with the data. Note that here we introduce an additional Green’s function, $G_s(b_s, y_3)$, which describes the development of the parton cascade within the rapidity interval y_3 between the triple Pomeron vertex (at $y_{\text{gap}} = -\ln \xi = Y - y_1$) and the new produced particle (placed at y_s and b_s in the rapidity and impact parameter plane); so $y_3 = y_{\text{gap}} - y_s$. This function

¹³ Here we have used the AGK cutting rules [26] for non-enhanced multi-Pomeron diagrams which, as was shown e.g. in [27], are valid for the perturbative QCD.

satisfies the same evolution equations (14) and (15) as G_j but with the initial conditions

$$\begin{aligned} G_{sii'}(b_s, 0) &= \lambda \left(1 - \sqrt{1 - G_i(b_s, y_{\text{gap}})} \right) \\ &\times \left(1 - \sqrt{1 - G_{i'}(b_s, y_{\text{gap}})} \right) \end{aligned} \quad (26)$$

and

$$k_{t;sii'}(b_s, 0) = \sqrt{k_{t,i}(b_s, y_{\text{gap}}) k_{t,i'}(b_s, y_{\text{gap}})}, \quad (27)$$

where $k_{t,i}$ and $k_{t,i'}$ are the values of k_t of the G–W components i and i' respectively.

The gap survival factors S^{eik} account for the incoming proton interactions

$$S_{ij}^{\text{eik}} = e^{-\Omega_{ij}(b_1+b_s, Y)/2} \quad (28)$$

while the value of $S_{ii'}^{\text{enh}}$ is given in terms of (23) as

$$S_{ii'}^{\text{enh}} = S_i^{\text{enh}}(b_s, Y - y_{\text{gap}}) S_{i'}^{\text{enh}}(b_s, Y - y_{\text{gap}}). \quad (29)$$

The corresponding opacity Ω_{si} can be calculated via

$$\exp(-\Omega_{si}(b_s, Y - y')) = 1 - G_i(b_s, Y - y').$$

3.4 Parton transverse momenta

In order to evaluate the characteristic transverse momenta of the secondaries produced at some rapidity y' we can multiply by $k_t(b, y')$ (15) the value of $G(b, y)$ for each G–W component j at $y = y'$ and then continue the evolution of this product $G_{(k_t),j}(b, y) = k_t(b, y')_j G_j(b, y)$ according to the master equation (14). The mean value $\langle k_t(y') \rangle$ is given by the ratio of ‘cross sections’ (say, (22)) calculated with $G_{(k_t),j}(b, y)$ to that calculated with the normal $G_j(b, y)$. Of course this $\langle k_t(y') \rangle$ is not equal to the mean momentum of the secondary hadrons, $\langle p_t \rangle$, which can be measured experimentally. The value of $\langle p_t \rangle$ will be modified by hadronization. However by looking at the energy, rapidity and b dependences of $\langle k_t \rangle$ we get some semi-quantitative understanding of the expected $\langle p_t \rangle$ behaviour.

3.5 Secondary Reggeon contributions

Besides the triple-Pomeron (PPP) term considered in Sect. 3.2 there are the contributions caused by secondary Reggeon (R) exchange. For relatively large ξ (that is not too large y_2) one has to account for the RRP term where the two upper Pomerons in Fig. 1b are replaced by R-exchange.

Assuming that the R-reggeons are emitted from valence quarks for all G–W eigenstates we put the *same* vertex couplings and form factors and write the corresponding exchange amplitude as

$$A_R(b) = 1 - e^{\Omega_R(b, y_2)/2} \quad (30)$$

with

$$\Omega_R(b, y_2) = \frac{\sigma_R e^{(\alpha_R(0)-1)y_2}}{4\pi B_R} e^{-b^2/4B_R}. \quad (31)$$

We take the intercept of the R-trajectory to be $\alpha_R(0) = 1/2$ and the slope $B_R = \alpha'_R y_2 + 2/0.71 \text{ GeV}^2$ with $\alpha'_R = 0.9 \text{ GeV}^{-2}$; the term $2/0.71$ corresponds to the dipole form factor $F_R(t) = 1/(1 - t/0.71)^2$.

Thus for the RRP contribution we obtain

$$\begin{aligned} \frac{\xi d\sigma^{RRP}}{d\xi} &= \int d^2 b_1 \sum_j |a_j|^2 \\ &\times \frac{G_j(b_1, y_1)}{\sigma_0} d^2 b_2 \left| \sum_i |a_i|^2 (1 - e^{-\Omega_R(b_2, y_2)/2}) \right. \\ &\times S_{ij}^{\text{eik}} S_i^{\text{enh}}(b_2, Y - y_2) \Big|^2, \end{aligned} \quad (32)$$

For very small ξ corresponding to low mass, M_X , dissociation the central Pomeron (in the lower part of Fig. 1) can be replaced by a R-reggeon. This forms the PPR term whose contribution decreases as $1/M_X \propto \exp(-y_1/2)$. However this, relatively low M_X , contribution in our case was accounted for within the G–W formalism. To obtain a more or less realistic behaviour at the lowest ξ end we assume resonance – ‘reggeon exchange’ duality and redistribute the low mass dissociation cross section given by (8) (minus the elastic cross section (7)) over y_1 with a $0.5 \exp(-y_1/2)$ weight.

In each case the corresponding t -slope was calculated as the mean value $\langle b_2^2 \rangle$.

3.6 Multiplicity distribution

The multiplicity distribution of charged hadrons observed in some rapidity interval is given by the convolution of several functions. First, this is the distribution of secondaries produced by one individual ‘cut’ Pomeron. It includes the distribution over the number of s -channel gluons and the effects of hadronization. Next we have the distribution over the number of Pomerons. Finally, the result may be affected by the ‘colour reconnection’ between the gluons from different Pomerons.

In the present model we neglect the colour reconnection effects and assume that the charged particles are emitted by one Pomeron according to Poisson’s law. To account for the charge conservation we take the Poisson over the number, $N_1 = N_1^+$, of positively charged particles. The element which will be studied below is the effect on the multiplicity distribution coming from the number, n , of the Pomerons.

In the one-channel eikonal approximation, that is for each G–W component, the distribution over the number of

Pomerons also takes a Poisson form

$$P_P(n) = \frac{\Omega^n(b)}{n!} e^{-\Omega(b)}, \quad (33)$$

where the mean number of the cut Pomerons, $\langle n \rangle = \Omega(b)$, depends on particular b value. That is actually we deal with the sum (integral) of a continuous number of Poissons with different $\langle n(b) \rangle$. This leads to the final distribution

$$\begin{aligned} P_h(N) &= \int w(b) \sum_n \frac{\Omega^n(b)}{n!} e^{-\Omega(b)} \\ &\times \frac{(n \cdot N_1)^N}{N!} e^{-n \cdot N_1} d^2 b, \end{aligned} \quad (34)$$

where the weight $w(b)$ is given by the integrand of the corresponding cross section. For non-diffractive inclusive events

$$w_{ij}(b) = \frac{1 - \exp(-\Omega_{ij}(b))}{\int d^2 b (1 - \exp(-\Omega_{ij}(b)))}$$

while for high-mass diffractive dissociation (22)

$$w_j = \frac{G_j(b_1, y_1) \int d^2 b_2 |\dots|^2}{\int d^2 b_1 G_j(b_1, y_1) \int d^2 b_2 |\dots|^2}, \quad (35)$$

where for simplicity we consider just a collision of a particular (i and j) G–W eigenstates; $|\dots|^2$ denotes the last two factors on the r.h.s. of (22). The $\Omega(b)$ which should be used in (34) is equal to $\Omega_j(b_1, y_1) = -\ln(1 - G_j(b_1, y_1))$.

4 Parameters of the model

Let us, first, discuss the expected reasonable values of the parameters of our model.

The free parameters which are used to tune the model are:

- The Regge intercept of the original (unscreened) Pomeron, $1 + \Delta$; from NLL BFKL we expect $\Delta \sim 0.2$.
- The initial value of the parton transverse momentum, $k_0 = k_t(b, y = 0)$. $1/k_0^2$ plays the role of the slope, α'_P , of the Pomeron trajectory. This slope is known to be rather small, say, $\alpha'_P = 0.25 \text{ GeV}^{-2}$ in the parametrization of [28]. Even a smaller $\alpha'_P = 0.14 \text{ GeV}^{-2}$ was obtained in [29]. Thus $k_0 \sim 2 \text{ GeV}$ looks to be reasonable value.
- Next, we have the elementary wee parton cross section, σ_0 , which should be of the order $2\pi/k_0^2 \sim 1 \text{ mb}$.
- Finally, we have the initial impact parameter distribution of the partons in each G–W eigenstate, which in our simplified model are described by a total of 6 parameters, as explained below.

Since we are looking mainly for the qualitative and semi-quantitative effects we try to be as simple as possible and take only two G–W components with equal weight $a_1 =$

Table 1 The values of the parameters in the two-channel eikonal fit to elastic pp ($p\bar{p}$) scattering data

Δ	0.17
σ_0 (GeV ⁻²)	1.18
k_0 (GeV)	2.2
$\lambda = g_{3P}/g_N$	0.2 (fixed)
f_1	11
d_1 (GeV ⁻²)	2.75
c_1 (GeV ²)	0.2
f_2	4.15
d_2 (GeV ⁻²)	1.3
c_2 (GeV ²)	0.3

$a_2 = 1/\sqrt{2}$. For each of these two G–W eigenstates the b dependence is parameterised by factors of the form

$$F_i(t) = \exp(-\sqrt{d_i(c_i - t)} + \sqrt{d_i c_i}), \quad (36)$$

where c_i is added to avoid a singularity at $t = 0$. Note that $F_i(0) = 1$. The starting distributions for the evolution in rapidity are

$$G_i(b, y = 0) = \frac{f_i}{4\pi} \int dt J_0(b\sqrt{|t|}) F_i(t). \quad (37)$$

Thus we have 3 free parameters (f_i which determines the value of the parton density, d_i and c_i) for each G–W eigenstate.

The values of parameters found to describe the data are listed in Table 1.

The first two parameters in Table 1 control the absolute value and the energy behaviour of the total cross section. k_0 is responsible for the shrinkage of diffractive cone, that is for velocity of diffusion in b space; while λ determines the probability of high mass diffractive dissociation. We fix $\lambda = 0.2$ to be equal to the value given by both – the analysis based on the perturbative QCD approach and the HERA data [31] and the triple-Regge analysis accounting for absorptive corrections [32]. The final 6 parameters define the parton densities and their b distribution in the two G–W eigenstates.

The parameters were tuned to reasonably describe the elastic pp ($p\bar{p}$) cross sections in the collider energy range as shown in Fig. 4. As a rule, when tuning the parameters, we use only two digits,¹⁴ since our goal is not to obtain the most precise description, but instead to achieve a qualitative understanding of the multi-Pomeron contributions and a semi-quantitative evaluation of the expected effects. In other words, we are seeking a general understanding of how high energy diffractive phenomena are driven by perturbative QCD. The fact that the values found for the parameters turn out to be in agreement with preliminary qualitative expectations gives support for the model.

¹⁴ Thus it may be possible to improve the description.

The resulting cross sections and elastic slope are presented in Table 2. Note that the model gives a reasonable probability of low-mass diffractive dissociation, $\sigma_{\text{lowM}}^{\text{SD}} = 3.75$ mb at $\sqrt{s} = 7$ TeV in agreement with the TOTEM, $\sigma_{\text{lowM}}^{\text{SD}} = 2.6 \pm 2.2$ mb, [30] measurement.

5 Results for diffractive dissociation

5.1 Cross section of single proton dissociation

The expected ξ behaviour of the cross section of single proton dissociation (SD) is shown in Fig. 7. The pure Pomeron component is shown by the dashed curve while the solid curve includes the secondary reggeon contribution (as described in Sect. 3.5). The black curves correspond to $\sqrt{s} = 13$ TeV. The result for $\sqrt{s} = 8$ TeV is shown by the thick blue curve. Here we use $\lambda = 0.2$ [31, 32] and $\sigma_R = 22$ mb which is consistent with the analysis of [32] and the secondary Reggeon contribution in the COMPETE fit [47, 48] of the pp total cross sections.

Recall that there is some tension between the points extracted by Goulianos and Montanha [49] from the CDF data and the cross sections of diffractive dissociation measured at the LHC. With $\lambda = 0.2$ we underestimate the CDF cross section at $\xi < 0.01$ (see Fig. 8) but overshoot a little the recent ATLAS [50] results (see [54] for a discussion).

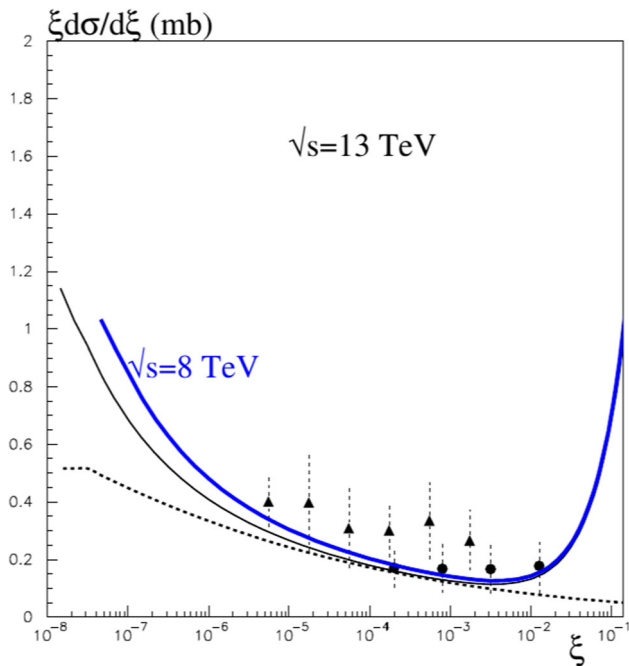
For $\xi < 0.01$ (where the RRP contribution becomes small) the value of $d\sigma^{\text{SD}}/d\ln\xi$ increases with decreasing ξ mainly due to the Pomeron intercept $1 + \Delta > 1$. However this growth is tamed by absorptive effects. At very small ξ , corresponding to low M_X , we see the contribution of the PPR term coming from G–W low-mass dissociation.

5.2 Rapidity distributions

We show in Fig. 9 the rapidity dependence of the charged particle densities dN_{ch}/dy expected in SD events in the central detector interval. Contrary to the standard plateau observed in this region in the non diffractive events the particle density dN_{ch}/dy in SD decreases when the rapidity of the secondary meson approaches the edge of the LRG (i.e. to the position of the triple-Pomeron vertex). This behaviour can be explained by looking at the product $G_j(b_1, y_s)G_{sii'}(b_s, y_3 = y_{\text{gap}} - y_s)$ in (25). Indeed, near the gap edge we deal with the beginning of the $G_{sii'}$ evolution where the particle density is rather small and the value $G_{sii'}$ increases rapidly. On the other hand the function $G_j(b_1, y_s)$ is already close to saturation and weakly depends on y_s (here y_s is large). Therefore the product $G_j(b_1, y_s)G_{sii'}(b_s, y_3 = y_{\text{gap}} - y_s)$ increases with y_3 , i.e. decreases when y_s approaches the gap edge y_{gap} .

Table 2 The predictions of the elastic and diffractive observables resulting from the description of the presently available data

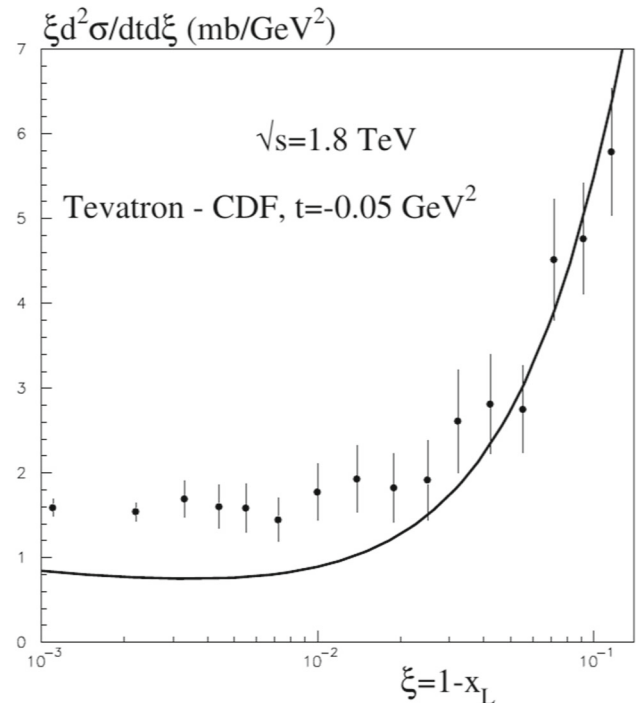
\sqrt{s} (TeV)	σ_{tot} (mb)	σ_{el} (mb)	$B_{\text{el}}(t=0)$ (GeV^{-2})	$\sigma_{\text{lowM}}^{\text{SD}}$ (mb)
0.0625	42.5	7.3	11.6	1.46
0.546	63.9	13.5	14.7	2.40
1.8	78.1	18.0	16.8	3.03
7	96.4	24.2	19.6	3.82
8	98.3	24.8	19.9	3.90
13	105.5	27.3	21.0	4.21

**Fig. 7** The ξ dependence of the single dissociation (SD) cross section at $\sqrt{s} = 13$ TeV (black). The dashed curve is the Pomeron component while the continuous curve includes the secondary Reggeon contribution. ATLAS (8 TeV) [50] and CMS (7 TeV) [51] data are shown by circles and triangles respectively. The CMS points have been reduced by a factor of 1.27 to approximately account for the fact that these data contain some admixture of double dissociation, in addition to pure SD [52]. Thick blue/upper curve corresponds to $\sqrt{s} = 8$ TeV. At $\xi > 3 \cdot 10^{-5}$ it is very close to the black curve

5.3 t dependence of SD cross section

The t -dependence of the SD amplitude can be calculated via the Fourier transform over the impact parameter b_2 (in (22)). Except for very small $|t|$ the distribution is rather close to a simple exponent (see Fig. 10 as an example).

The value of the slope expected in proton diffractive dissociation is shown in Fig. 11. Note that the secondary Reggeon terms enter with a very large slope $B_{\text{dis}}(t=0)$ (up to 40 GeV^{-2} at $\xi = 10^{-3}$). Therefore for $\xi \gtrsim 0.003$ (where the role of the secondary RRP contribution becomes important) the value of B_{dis} increases with ξ . The large value of B_{dis} in RRP term is explained by strong absorption which pushes

**Fig. 8** The comparison of the model with the results of the analyses by Goulianos and Montanha of the CDF data [49] at $\sqrt{s} = 1.8$ TeV and $t = -0.05 \text{ GeV}^2$

the PPR and RRP contributions to the far periphery of the disk. So, only the large b_2 tail survives.

On the other hand the slope corresponding to the pure Pomeron-induced dissociation is smaller ($B_{\text{dis}} \simeq 7 \text{ GeV}^{-2}$ at $\xi = 10^{-3}$). In this case the large b_1 needed to go to the periphery of the disk is mainly provided by a large b_1 corresponding to the central (in Fig. 1) “inelastic” (cut) Pomeron while the value of b_2 (responsible for the interaction across the LRG) stays rather small. If we neglect the enhanced diagrams in Fig. 5 then we get $B_{\text{dis}} \simeq 5 \text{ GeV}^{-2}$ (at $\xi = 10^{-4} - 10^{-3}$). Only the S^{enh} survival factor allows a larger B_{dis} up to $7-8 \text{ GeV}^{-2}$ by absorbing part of the low- b_2 contribution.

The growth of B_{dis} at very small ξ is due to the slope of the effective Pomeron trajectory, $\alpha'_{p,\text{eff}}$, (i.e. expansion of the disk in b space) and the PPR term which describes low-mass dissociation. We emphasize that in Fig. 11 we have plotted the slope at $t = 0$, which is larger than the mean slope B_{dis}

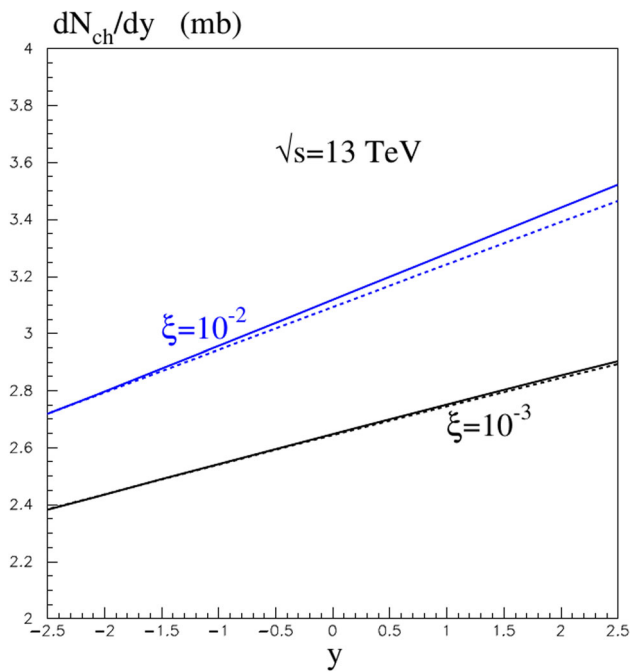


Fig. 9 The rapidity dependence of the charged multiplicity observed in the central detector for SD events with $\xi = 0.01$ (blue) and 0.001 (black) at $\sqrt{s} = 13$ TeV. The dashed curves correspond to the pure Pomeron-induced cross section without the secondary Reggeon contribution

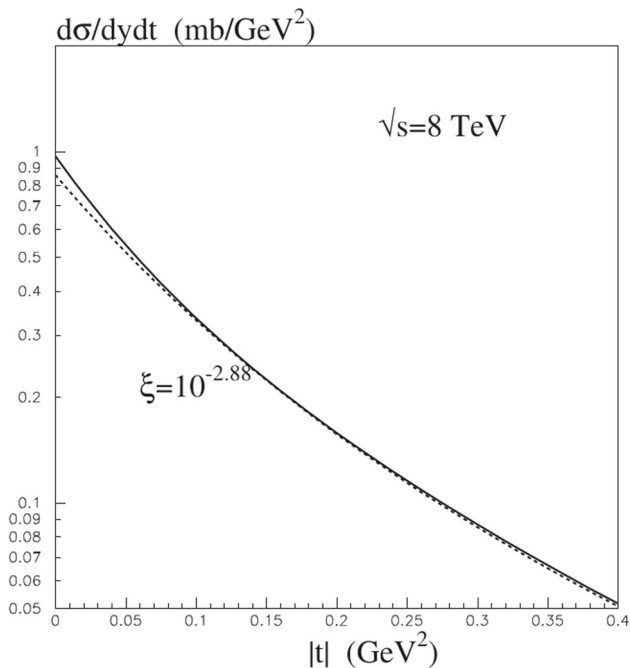


Fig. 10 The t dependence of the SD cross section $d\sigma/dydt$ at $\sqrt{s} = 8$ TeV and $\xi = 10^{-2.88}$ (this value of ξ is chosen to compare with the ATLAS-ALFA [50] results at $\langle \xi \rangle = 10^{-2.88}$). The dashed curve corresponds to the pure Pomeron-induced cross section without the secondary Reggeon contribution

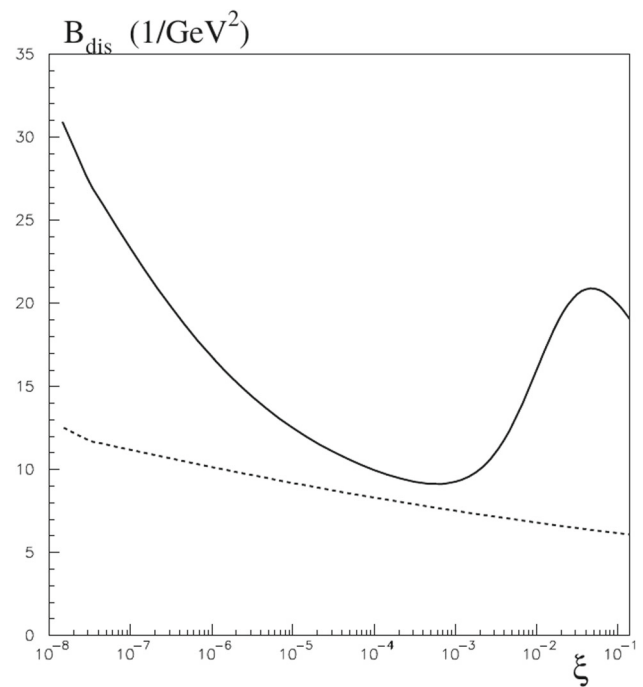


Fig. 11 The ξ dependence of the t -slope $B_{\text{dis}}(t = 0)$ in the single proton dissociation process at $\sqrt{s} = 13$ TeV. The dashed curve is the Pomeron component while the continuous curve includes secondary Reggeon contributions. Note that here we show the slope at $t = 0$. As it is seen from Fig. 10 the mean slope (within a larger $|t|$ interval) is a bit smaller

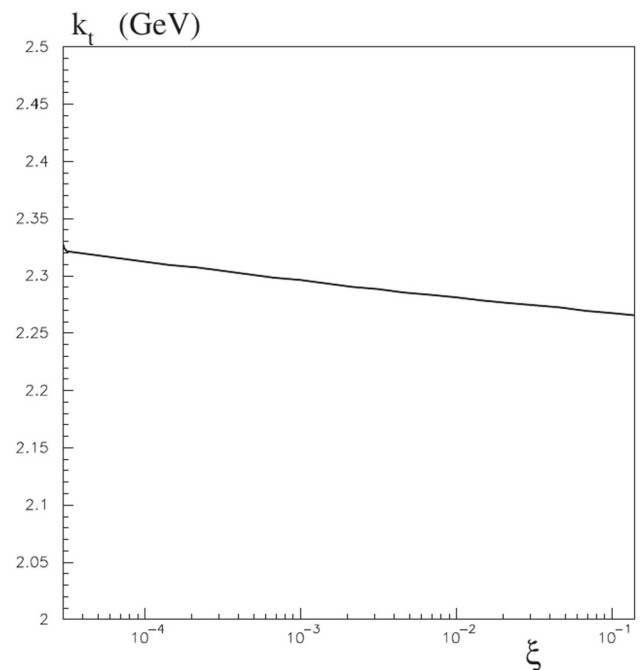


Fig. 12 The ξ behaviour of the characteristic transverse momentum k_t measured at $\eta = 0$ (in the laboratory frame, i.e. the pp centre of mass, system) in single proton dissociation at $\sqrt{s} = 13$ TeV

fitted in some finite t -interval. In particular at $\sqrt{s} = 8$ TeV and $\xi = 10^{-2.88}$ the mean slope ‘measured’ between $|t| = 0.02$ and 0.32 GeV² is $B_{\text{mean}}(0.02 - 0.32) = 7.6$ GeV⁻² while the value of $B_{\text{dis}}(t = 0) = 10.3$ GeV⁻².

Formally we have the possibility to introduce some additional slope B_{3P} of the triple-Pomeron vertex. However its natural value should be $B_{3P} \sim 1/k_0^2 \sim 0.25$ GeV⁻² which is rather small. On the other hand the value of k_0 controls the shrinkage of the diffractive cone and it is needed to keep $k_0 \sim 2$ GeV in order to reproduce the available elastic $d\sigma_{el}/dt$ data.

Finally, we show in Fig. 12 the typical wee-parton transverse momentum at $\eta_{Lab} = 0$ (that is near the centre of mass of the two colliding protons). Note that $k_t(\xi)|_{\eta=0}$ weakly increases with decreasing ξ , but still remains close to its initial value $k_0 = 2.2$ GeV. This means that in the diffracted system X we expect the transverse momentum distribution of secondaries and the mean value of $\langle p_t \rangle$ to be close to that observed at comparatively low (say, $\sqrt{s} \sim 20$ – 40 GeV) energies. The explanation is evident. The dissociation comes mainly from the periphery of the disk where the parton density is small. Thus, far from the saturation limit there is no reason to noticeably enlarge k_t . Recall that in non-diffractive inclusive events we get at $\sqrt{s} = 13$ TeV a larger $k_t(\eta = 0) = 2.73$ GeV.

Note that here we consider the secondaries produced somewhere in the centre of the M_X system and not too close to the edge of LRG. Near the edge of LRG the situation is more interesting and complicated. Recall that the Pomeron has a small transverse size (see e.g. [5,53]). In comparison with the proton radius ~ 1 fm the Pomeron size is $\sim 1/k_0 \sim 0.1$ fm. This is indicated by the small value of the slope of the Pomeron trajectory $\alpha'_P \leq 0.25$ GeV⁻² (see e.g. [28,55,56])¹⁵ and the very small (consistent with zero) t -slope of the triple-Pomeron vertex (see e.g. [32,57,58]).¹⁶ Therefore, in comparison with the proton fragmentation region in ‘Pomeron fragmentation’ (i.e. near the edge of the LRG) we expect a larger mean transverse momenta, p_t , and a broader p_t distribution of the secondaries. Some indication in favour of this can be seen in Fig. 2 of [1] where in comparison with the PYTHIA 8 Monte Carlo simulations the particle density increases with p_t . The

¹⁵ It was shown long ago in terms of the multiperipheral models [24] and in terms of the parton cascade [7] that the value of $\alpha' \propto 1/k_t^2$ where k_t is the typical transverse momentum of the partons (t -channel propagators in the case of multiperipheral models). Simultaneously this value of k_t determines the size of the bound system which forms the Regge pole (Pomeron).

¹⁶ In these papers the triple Pomeron vertex was extracted fitting rather old CERN-ISR data (Tevatron data was included in [32]). However this energy was sufficient to determine the triple-Pomeron contribution and since the vertex occupies a limited rapidity interval we can use the obtained results at larger energies, in particular for the LHC region.

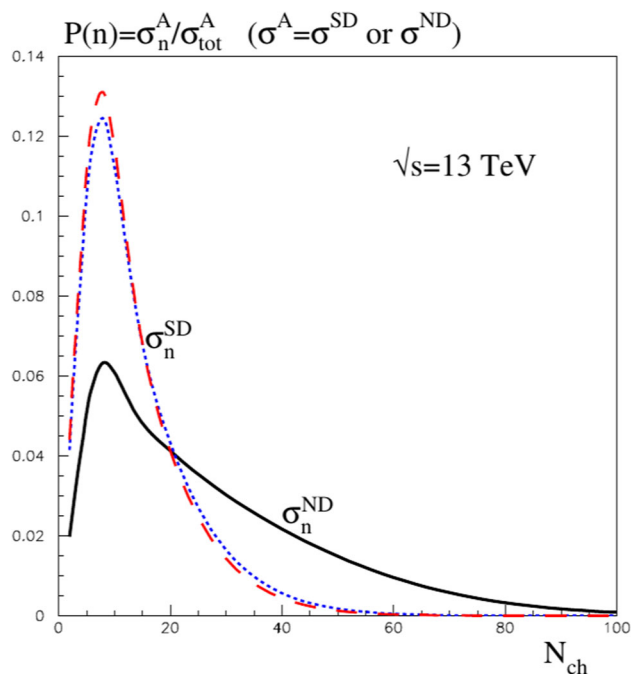


Fig. 13 The distribution over the charged hadron multiplicity in non-diffractive (ND) events (continuous curve) and in the case of single proton (SD) dissociation at $\sqrt{s} = 13$ TeV for $\xi = 10^{-3}$ (red long-dashed curve) and $\xi = 10^{-2}$ (blue short-dashed curve). (We assume that mean number of charged hadrons emitted by *one* cut Pomeron is equal to 8 in the rapidity interval that the value of N_{ch} was measured)

‘data/MC’ ratio exceeds 1 and reaches about 2 for $p_t > 1$ GeV.

Recall also that the Pomeron consists mainly of gluons and so the Pomeron is essentially a singlet with respect to the flavour SU(3) group. Therefore, it would be interesting to observe in the Pomeron fragmentation region (close to the edge of the LRG) the presence of η and η' mesons. Since η' is almost a singlet of flavour SU(3) and contains a large gluon component we may expect that the Pomeron fragmentation region will be enriched by η' mesons. Besides this, there should be a good chance to observe 0^{++} and 2^{++} glueballs in the Pomeron fragmentation region.

5.4 Multiplicity distribution

As explained in Sect. 5.4 the expected multiplicity distribution is represented by the sum (integral) of ‘Poissons’ with different mean $\langle N_{ch} \rangle$ which depends on the particular impact parameter and the number of cut Pomerons. Since diffractive dissociation events survive only in the region where the probability of multiple parton interactions is small (and correspondingly the multi-Pomeron contributions are suppressed) we expect in these events a smaller multiplicity and a rather narrow distribution.

Indeed, as seen in Fig. 13, in non-diffractive events we observe a long high N_{ch} tail caused by the integration over a

large interval of impact parameters b ; at each value of b we deal with a different number of cut Pomerons $\langle n \rangle = \Omega(b)$. On the other hand the dissociation events come from the edge of disk where $\Omega \leq 1$. Therefore here the distribution is much narrower and the mean multiplicity is about twice smaller ($\langle N_{\text{ch}}^{\text{dis}} \rangle = 13.3$ for $\xi = 10^{-3}$ and $\sqrt{s} = 13$ TeV instead of $\langle N_{\text{ch}}^{\text{dis}} \rangle = 27.5$ for the non-diffractive case).

6 Discussion

In the previous sections we have studied single diffractive (SD) processes and shown qualitative (semi-quantitative) effects caused by the fact that at small b stronger absorptive corrections push the amplitude of dissociation to the periphery of the disk. In comparison with [59], where the diffusion in b space was neglected and $\alpha'_p = 0$ was assumed, here we pay the most attention just to the possibility that partons move in b plane. On the other hand, in [59] the diffusion in $\ln k_t$ was accounted for more precisely. In the present model we consider just the evolution (with rapidity) at a typical value of k_t . However, since on the periphery of disk, from which the major SD contribution comes, the parton density is relatively small and the value of k_t practically does not change we believe that the present model is more appropriate for analysis of the SD processes.

Acknowledgements We thank Kenneth Osterberg, Paul Newman, Valery Schegelsky and Marek Tasevsky for discussions. MGR thanks the IPPP at the University of Durham for hospitality.

Data Availability Statement This manuscript has no associated data or the data will not be deposited. [Authors' comment: There are no external data associated with the manuscript.]

Open Access This article is licensed under a Creative Commons Attribution 4.0 International License, which permits use, sharing, adaptation, distribution and reproduction in any medium or format, as long as you give appropriate credit to the original author(s) and the source, provide a link to the Creative Commons licence, and indicate if changes were made. The images or other third party material in this article are included in the article's Creative Commons licence, unless indicated otherwise in a credit line to the material. If material is not included in the article's Creative Commons licence and your intended use is not permitted by statutory regulation or exceeds the permitted use, you will need to obtain permission directly from the copyright holder. To view a copy of this licence, visit <http://creativecommons.org/licenses/by/4.0/>.
Funded by SCOAP³.

References

1. L. Fulek (for the STAR Collaboration) [arXiv:1906.04963](https://arxiv.org/abs/1906.04963) [hep-ex]
2. A.M. Sirunyan et al, (CMS and TOTEM) [arXiv:2002.12146](https://arxiv.org/abs/2002.12146)
3. G. Aad et al. (ATLAS) [arXiv:1911.00453](https://arxiv.org/abs/1911.00453)
4. V.N. Gribov, Sov. Phys. JETP **26**, 414 (1968)
5. V.A. Khoze, A.D. Martin, M.G. Ryskin, J. Phys. G **46**, 11LT01 (2019). [arXiv:1907.04603](https://arxiv.org/abs/1907.04603)
6. R.P. Feynman, Phys. Rev. Lett. **23**, 1415 (1969)
7. V.N. Gribov, Space-time description of hadron interactions at high-energies. Lecture at the 1973 LNPI Winter School. [arXiv:hep-ph/0006158](https://arxiv.org/abs/hep-ph/0006158)
8. V.S. Fadin, E.A. Kuraev, L.N. Lipatov, Phys. Lett. **60B**, 50 (1975)
9. E.A. Kuraev, L.N. Lipatov, V.S. Fadin, Sov. Phys. JETP **44**, 443 (1976)
10. E.A. Kuraev, L.N. Lipatov, V.S. Fadin, Zh. Eksp. Teor. Fiz. **71**, 840 (1976)
11. E.A. Kuraev, L.N. Lipatov, V.S. Fadin, Sov. Phys. JETP **45**, 199 (1977)
12. E.A. Kuraev, L.N. Lipatov, V.S. Fadin, Zh. Eksp. Teor. Fiz. **72**, 377 (1977)
13. I.I. Balitsky, L.N. Lipatov, Sov. J. Nucl. Phys. **28**, 822 (1978)
14. I.I. Balitsky, L.N. Lipatov, Yad. Fiz. **28**, 1597 (1978)
15. L.V. Gribov, E.M. Levin, M.G. Ryskin, Phys. Rep. **100**, 1 (1983)
16. E.M. Levin, M.G. Ryskin, Phys. Rep. **189**, 267 (1990)
17. V.A. Khoze, M.G. Ryskin, M. Tasevsky, Chapter 20 in P.A. Zyla et al. [Particle Data Group], PTEP **2020**(8), 083C01 (2020)
18. M.L. Good, W.D. Walker, Phys. Rev. **120**, 1855 (1960)
19. V.S. Fadin, L.N. Lipatov, Phys. Lett. B **429**, 127 (1998). [arXiv:hep-ph/9802290](https://arxiv.org/abs/hep-ph/9802290)
20. M. Ciafaloni, G. Camici, Phys. Lett. B **430**, 349 (1998). [arXiv:hep-ph/9803389](https://arxiv.org/abs/hep-ph/9803389)
21. G.P. Salam, JHEP **9807**, 019 (1998). [arXiv:hep-ph/9806482](https://arxiv.org/abs/hep-ph/9806482)
22. M. Ciafaloni, D. Colferai, Phys. Lett. B **452**, 372 (1999). [arXiv:hep-ph/9812366](https://arxiv.org/abs/hep-ph/9812366)
23. S.J. Brodsky et al., JETP Lett. **70**, 155 (1999)
24. E.L. Feinberg, D.S. Chernavski, Usp. Fiz. Nauk **82**, 41 (1964)
25. V.N. Gribov, Yad. Fiz. **9**, 640 (1969) [Sov. J. Nucl. Phys. **9**, 369 (1969)]
26. V.A. Abramovsky, V.N. Gribov, O.V. Kancheli, Yad. Fiz. **18**, 595 (1973) [Sov. J. Nucl. Phys. **18** (1974) 308]
27. J. Bartels, M.G. Ryskin, Z. Phys. C **76**, 241 (1997). [arXiv:hep-ph/9612226](https://arxiv.org/abs/hep-ph/9612226)
28. A. Donnachie, P.V. Landshoff, Nucl. Phys. B **231**, 189 (1984)
29. J.P. Burg et al., Nucl. Phys. B **217**, 285 (1983)
30. TOTEM Collaboration, G. Antchev et al., Eur. Phys. Lett. **101**, 21003 (2013)
31. E.G. de Oliveira, A.D. Martin, M.G. Ryskin, Phys. Lett. B **695**, 162–164 (2011)
32. E.G.S. Luna, V.A. Khoze, A.D. Martin, M.G. Ryskin, Eur. Phys. J. C **59**, 1 (2009). [arXiv:0807.4115](https://arxiv.org/abs/0807.4115) [hep-ph]
33. TOTEM Collaboration, G. Antchev et al., Europhys. Lett. **101**, 21002 (2013)
34. TOTEM Collaboration, G. Antchev et al., Eur. Phys. J. C **79**, 861 (2019)
35. TOTEM Collaboration, G. Antchev et al., Eur. Phys. J. C **80**, 91 (2020)
36. UA4 Collaboration, M. Bozzo et al., Phys. Lett. B **147**, 385 (1984)
37. UA4/2 Collaboration, C. Augier et al., Phys. Lett. B **316**, 448 (1993)
38. UA1 Collaboration, G. Arnison et al., Phys. Lett. B **128**, 336 (1982)
39. E710 Collaboration, N.A. Amos et al., Phys. Lett. B **247**, 127 (1990)
40. C.D.F. Collaboration, F. Abe et al., Phys. Rev. D **50**, 5518 (1994)
41. N. Kwak et al., Phys. Lett. B **58**, 233 (1975)
42. U. Amaldi et al., Phys. Lett. B **66**, 390 (1977)
43. L. Baksay et al., Nucl. Phys. B **141**, 1 (1978)
44. U. Amaldi et al., Nucl. Phys. B **166**, 301 (1980)
45. M. Bozzo et al., Phys. Lett. B **155**, 197 (1985)
46. D0 Collaboration, V.M. Abazov et al., Phys. Rev. D **86**, 012009 (2012)
47. J.R. Cudell et al., COMPETE Collaboration, Phys. Rev. Lett. **89**, 201801 (2002). [arXiv:hep-ph/0206172](https://arxiv.org/abs/hep-ph/0206172)

48. C. Patrignani et al. [Particle Data Group], *Chin. Phys. C* **40**(10), 100001 (2016) (**Section 51**)
49. K.A. Goulianos, J. Montanha, *Phys. Rev. D* **59**, 114017 (1999). [arXiv:hep-ph/9805496](#)
50. G. Aad et al. (ATLAS Collaboration), *JHEP* **2002**, 042 (2020) [Erratum *JHEP*10 (2020) 182]. [arXiv:1911.00453](#) [hep-ex]
51. V. Khachatryan (CMS Collaboration), *Phys. Rev. D* **92**, 012003 (2015). [arXiv:1503.08689](#) [hep-ex]
52. P. Newman, M. Tasevsky, private communication
53. M.G. Ryskin, A.D. Martin, V.A. Khoze, *J. Phys. G* **38**, 085006 (2011). [arXiv:1105.4987](#) [hep-ph]
54. V.A. Khoze, A.D. Martin, M.G. Ryskin, *Int. J. Mod. Phys. A* **30**, 1542004 (2015). [arXiv:1402.2778](#) [hep-ph]
55. V.A. Khoze, A.D. Martin, M.G. Ryskin, *Eur. Phys. J. C* **73**, 2503 (2013). [arXiv:1306.2149](#) [hep-ph]
56. E. Gotsman, E. Levin, U. Maor, *Int. J. Mod. Phys. A* **30**(08), 1542005 (2015). [arXiv:1403.4531](#) [hep-ph]
57. A.B. Kaidalov, V.A. Khoze, Y.F. Pirogov, N.L. Ter-Isaakyan, *Phys. Lett.* **45B**, 493 (1973)
58. R.D. Field, G.C. Fox, *Nucl. Phys. B* **80**, 367 (1974)
59. M.G. Ryskin, A.D. Martin, V.A. Khoze, *Eur. Phys. J. C* **71**, 1617 (2011). [arXiv:1102.2844](#) [hep-ph]